Journal of Power Sources 324 (2016) 704–711

Contents lists available at ScienceDirect

Journal of Power Sources

journal homepage: www.elsevier.com/locate/jpowsour

Improving sulfolane-based electrolyte for high voltage Li-ion cells with electrolyte additives

Jian Xia, J.R. Dahn*

Dept. of Physics and Atmospheric Science, Dalhousie University, Halifax, Nova Scotia, B3H3J5, Canada

HIGHLIGHTS

- Sulfolane:ethylmethyl carbonate-based electrolytes with additives are studied.
- The additive combination of vinylene carbonate and tri-allyl phosphate is best.
- $Li(Ni_{0.4}Mn_{0.4}Co_{0.2})O_2$/graphite cells with such electrolytes operate well to 4.5 V.

ARTICLE INFO

Article history:
Received 8 January 2016
Received in revised form
22 May 2016
Accepted 1 June 2016
Available online 6 June 2016

Keywords:
Sulfolane-based electrolyte
Electrolyte additives
Vinylene carbonate
Tri-allyl phosphate
High voltage Li-ion cells

ABSTRACT

An electrolyte mixture containing 1 M $LiPF_6$ in sulfolane:ethylmethyl carbonate 3:7 with vinylene carbonate and other electrolyte additives exhibited promising cycling and storage performance in high voltage $Li(Ni_{0.4}Mn_{0.4}Co_{0.2})O_2$/graphite pouch type Li-ion cells tested to 4.5 V. Voltage drop during storage, coulombic efficiency, charge endpoint capacity slippage during ultra high precision cycling, charge-transfer resistance after storage or cycling, gas evolution during storage and cycling as well as capacity retention during long-term cycling were examined. The results for cells with sulfolane-based electrolytes were compared with those for cells with ethylene carbonate-based electrolytes containing state-of-the-art electrolyte additives. This survey showed that the combination of vinylene carbonate and triallyl phosphate as electrolyte additives in sulfolane:ethylmethyl carbonate electrolyte yielded cells capable of better performance during tests to 4.5 V than cells with ethylene carbonate-based electrolytes. These results suggest that sulfolane-based electrolytes may be promising for high voltage Li-ion cells.

1. Introduction

Li-ion batteries have been extensively used as power sources in applications such as mobile devices, electric vehicles (EVs), hybrid EVs (HEVs) and grid energy storage. Improvements in energy density as well as cycle or calendar lifetime are desired for these applications [1]. While the lifetime of all Li-ion cells can be improved by using suitable electrolyte additives, the energy density depends on the choice of electrode materials [2,3]. Efforts to increase energy density have led to the development of positive and negative electrode materials with higher specific capacities as well as the positive electrode materials with a higher average potential vs Li/Li^+. Some high potential positive electrode materials have been developed such as $LiCoPO_4$ [4,5], Li_2CoPO_4F [6], $Li_3V_2(PO_4)_3$ [7], $LiNi_{0.5}Mn_{1.5}O_4$ [8], and $Li[Ni_xMn_xCo_{1-2x}]O_2$ [9]. Long-term performance of Li-ion cells operating to potentials above 4.4 V has been poor due to increased electrolyte oxidation at the surface of positive electrode as the potential increases [10–12]. These issues with Li-ion cells, even incorporating state of the art electrolytes, begin to appear at 4.3 V [13] and become very problematic at or above 4.5 V during cell operation [14,15].

One solution to the electrolyte oxidation problem is to find new alternative electrolyte formulations with high anodic stability. Sulfone-based electrolytes have been developed since they have high dielectric constant and high electrochemical oxidation potential compared with carbonate-based electrolytes [16–20]. However, sulfone-based electrolytes also suffer from their high melting point, high viscosity and most importantly inability to passivate the graphite electrode well. Therefore, a secondary solvent that can decrease viscosity and proper electrolyte additives that can passivate the graphite electrode are needed. Recently, Xia et al. [21] demonstrated an electrolyte system composed of sulfolane (SL), ethylmethyl carbonate (EMC) and vinylene carbonate

* Corresponding author.
E-mail address: jeff.dahn@dal.ca (J.R. Dahn).

http://dx.doi.org/10.1016/j.jpowsour.2016.06.008
0378-7753/

(VC) which showed good cycling and storage performance in NMC442/graphite Li-ion pouch cells. Problems with SL:EMC:VC electrolyte are gas evolution during cycling and storage at high temperatures. Therefore, it is quite crucial and interesting to find electrolyte additives which could function as a gas reducer in SL:EMC electrolytes and, when used together with VC, are competitive or better than state-of-the-art EC-based electrolytes containing electrolyte additives.

Some sulfur containing additives such as prop-1-ene-1,3-sultone (PES) [22,23], methylene methanedisulfonate (MMDS) [24] and trimethylene sulfate (TMS) [25] have been shown to be good gas reducers in NMC111/graphite Li-ion pouch cells. The beneficial effect of these additives is enhanced when combined with a third electrolyte additive, namely, tris(trimethylsilyl) phosphite (TTSPi). Several combinations have shown good storage and cycling performance as well as improved safety features in both NMC111/graphite and NMC442/graphite Li-ion pouch cells [26–28]. Beside these sulfur-containing additives, triallyl phosphate (TAP) was also studied as a good gas reducer at high temperatures in NMC442/graphite pouch cells [29]. When TAP was used together with PES, gas evolution was further decreased while the cycling and storage performance were improved [30].

In this paper, the SL:EMC:VC solvent mixtures with various different electrolyte additives were studied in NMC442/graphite Li-ion pouch cells. Experiments were made using Ultra High Precision Coulometry (UHPC) [31], a precision storage system [32], an *ex-situ* gas evolution apparatus [33] as well as electrochemical impedance spectroscopy (EIS) [34]. Long-term cycling results were also conducted to compare the SL:EMC:VC electrolyte system with EC-based electrolyte systems containing some promising additive blends.

2. Experimental

1 M $LiPF_6$ EC/EMC (3:7 wt% ratio, BASF, 99.99%) was used as the control electrolyte. 1 M $LiPF_6$ Sulfolane/EMC (3:7 wt% ratio) was used as the studied electrolyte. The sulfolane was obtained from Novolyte Technologies, now BASF (99.99% pure with 9.2 ppm water). The additives were added at 1–8 wt% to the studied electrolyte. These additives included vinylene carbonate (VC), prop-1-ene,1,3-sultone (PES), methylene methanedisulfonate (MMDS), ethylene sulfite (ES), Propanediol cyclic sulfate (trimetylene sulfate - TMS), 1,3,2-dioxathiolan-2,2-oxide (ethylene sulfate - DTD), tris trimethylsilyl phosphite (TTSPi) as well as triallyl phosphate (TAP). Fig. S1a (supporting information) shows the chemical structure of additives that were studied in this paper. The reasons for choosing these additives are explained in Refs. [26] and [29]. The purities and the suppliers of the additives used are listed in Table 1 (supporting information). Some promising electrolyte additive combinations in 1 M $LiPF_6$ EC:EMC (3:7 by wt.) electrolyte include 2% PES + 1% MMDS (or DTD) + 1% TTSPi (PES211) and 2% PES + 2%TAP were also used for comparison in some of the experiments. The details of the PES211 electrolyte have been reported in Ref. [14].

The 402035-size pouch cells employed in this study were all Li$[Ni_{0.4}Mn_{0.4}Co_{0.2}]O_2$ (NMC442)/graphite cells with a capacity of 245 mAh balanced for 4.7 V operation. Fig. S2 shows SEM images of the top surfaces of the NMC442 and graphite electrodes so that readers can appreciate the morphology of the particles that make up the electrodes. The cells were produced by Li-Fun Technology (Xinma Industry Zone, Golden Dragon Road, Tianyuan District, Zhuzhou City, Hunan Province, PRC, 412000). The pouch cells were vacuum sealed without electrolyte in China and then shipped to our laboratory in Canada. Details about the electrode loadings, thicknesses, compressed electrode density, separator, etc., can be found in Ref. [35].

Before filling with electrolyte, the cells were cut just below the heat seal and dried at 80 °C under vacuum for 14 h to attempt to remove residual water. Then the cells were transferred immediately to an argon-filled glove box for filling and vacuum sealing. The NMC442/graphite pouch cells were filled with 0.75 mL of electrolyte (0.90 g for EC:EMC 3:7 electrolyte and 0.86 g for SL:EMC 3:7 electrolyte). After filling, cells were vacuum-sealed with a compact vacuum sealer (MSK-115A, MTI Corp.). First, cells were placed in a temperature box at 40 °C where they were held at 1.5 V for 24 h, to allow for the completion of wetting. Then, cells were charged at 12 mA (C/20) to 3.5 V. This step is called formation step 1. After Formation step 1, cells were transferred into the glove box, cut open to release any gas generated and vacuum sealed again. These cells were then charged again from 3.5 V at 12 mA (C/20) to 4.5 V. This step is called formation step 2. After formation step 2, the cells were transferred into the glove box, cut open to release gas generated and then vacuum sealed again. These degassing voltages were selected based on the in-situ gas evolution experiments that show most of the gas evolves in the formation step at voltages below 3.5 V and above 4.3 V [36]. After the two degassing processes, cells were then discharged to 3.8 V where impedance spectra were measured.

The cycling/storage procedure was carried out using the Ultra High Precision Charger (UHPC) at Dalhousie University [31]. Testing was between 2.8 and 4.4 V at 40 ± 0.1 °C. Cells were first charged to 4.400 V using currents corresponding to C/10, stored open circuit at 4.400 V for 20.00 h and then discharged to 2.800 V using currents corresponding to C/10. This process was repeated on the UHPC for 15 cycles where comparisons were made. The cycling/storage procedure was designed so that the cells were exposed to higher potentials for significant fractions of their testing time [37]. For storage experiments, cells were first discharged to 2.8 V and charged to 4.5 V two times. Then the cells were held at 4.5 V until the measured current decreased to 0.0025 C. A Maccor series 4000 cycler was used for the preparation of the cells prior to storage. After the pre-cycling process, cells were carefully moved to the storage system which monitored their open circuit voltage every 6 h during a total storage time of 500 h. Storage experiments were made at both 40 and 60 °C.

Ex-*situ* (static) gas measurements were used to measure gas evolution during formation and during cycling [33]. The measurements were made using Archimedes' principle with cells suspended from a balance while submerged in liquid. The changes in the weight of the cell suspended in fluid, before and after testing are directly related to the volume changes through the change in the buoyant force. The change in mass of a cell, Δm, suspended in a fluid of density, ρ, is related to the change in cell volume, Δv, by

$$\Delta v = -\Delta m/\rho \quad (1)$$

Ex-situ measurements were made by suspending pouch cells from a fine wire "hook" attached under a Shimadzu balance (AUW200D). The pouch cells were immersed in a beaker of de-ionized "nanopure" water (18.2 MΩ) that was at 20. ± 1 °C for measurement.

Electrochemical impedance spectroscopy (EIS) measurements were conducted on NMC111/graphite pouch cells after formation and also after cycling on the UHPC [34]. Cells were charged or discharged to 3.80 V before they were moved to a 10 ± 0.1 °C temperature box. Alternating current (AC) impedance spectra were collected with ten points per decade from 100 kHz to 10 mHz with a signal amplitude of 10 mV at 10 ± 0.1 °C. A Biologic VMP-3 was used to collect these data.

3. Results and discussion

Fig. 1a–b shows the differential capacity (dQ/dV) vs. V curves for NMC442/graphite pouch cells with some binary and ternary additive combinations in the SL:EMC electrolyte system during formation step 1. From the dQ/dV vs. V curves, one can determine at which potential the additives or solvents initially react with the graphite electrode. The control cells (1 M $LiPF_6$ in EC:EMC 3:7) showed a pronounced peak at 3.0 V which corresponds to a potential of about 0.65 V vs. Li/Li^+. When 2% VC was added to the control electrolyte, the peak shifted to a lower potential of about 2.9 V which corresponds to about 0.75 V vs. Li/Li^+. The dQ/dV vs. V curve of the cells with 2% VC in SL:EMC system showed a small peak around 2.70 V (0.95 V vs. Li/Li^+). When one more additive was added to the SL:EMC:VC system, the peak position was dominated by reduction of the new additive on the graphite surface. For example, the reduction potentials for the additives MMDS, PES, ES, DTD, TAP and TMS in SL:EMC:VC system are 2.40 V (1.25 V vs. Li/Li^+), 2.45 V (1.20 V vs. Li/Li^+), 2.50 V (1.15 V vs. Li/Li^+), 2.50 V (1.15 V vs. Li/Li^+), 2.65 V (1.00 V vs. Li/Li^+) and 2.70 V (0.95 V vs. Li/Li^+), respectively. Table 2 (Supporting information) compares the initial reduction potential vs. Li/Li^+ of these additives in SL:EMC and EC:EMC electrolytes. Table 2 shows that the initial reduction potential of these additives changes somewhat with the solvents. Fig. 1b shows that adding a third additive, TTSPi, to the some of the binary electrolyte additive systems, does not change the dQ/dV vs. V curve in a substantial way, suggesting TTSPi does not impact the reduction of the additives as determined in Fig. 1a.

Fig. 2 shows typical data collected during some of these experiments. Two electrolyte systems including 2% PES +1% MMDS +1% TTSPi in EC:EMC and 2% VC + 2% TAP in SL:EMC were selected for comparison in Fig. 2. Fig. 2a shows typical open circuit voltage (OCV) vs. time during 500 h storage at 60 ± 0.1 °C for NMC442/graphite cells in using the two electrolyte systems. The voltage drop (V_{drop}) during storage indicates the occurrence of electrolyte oxidation at the positive electrode and has been shown to correlate

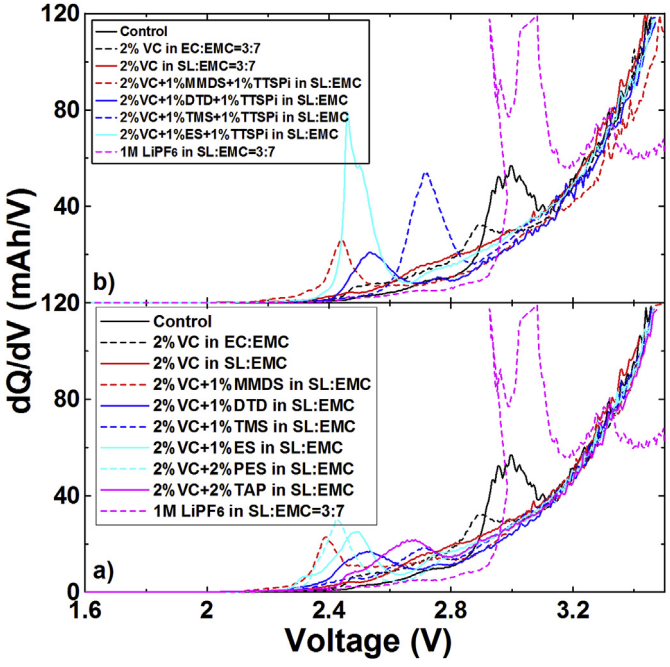

Fig. 1. Differential capacity (dQ/d*V*) vs. potential (*V*) during formation step 1 for the 240 mAh NMC442/graphite pouch cells containing SL:EMC electrolyte with a) binary additive combinations and b) ternary additive combinations as indicated.

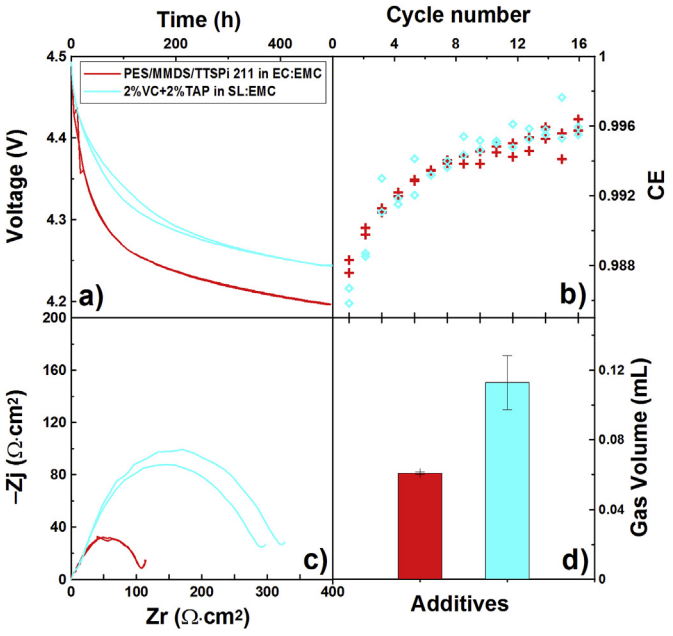

Fig. 2. a) Open circuit voltage vs. time during 500 h storage at 60 °C (initial potential was 4.5 V); b) Coulombic efficiency during UHPC cycling (C/10 to 4.4 V, 20 h OCV, C/10 discharge to 2.8 V–40 °C), c) Nyquist plots after UHPC cycling (10 °C and 3.8 V) and d) gas evolution during UHPC cycling at 40.°C for NMC442/graphite pouch cells with different electrolyte additives as indicated. Fig. 2 gives example data showing the methods used in this paper.

well with charge endpoint capacity slippage [32]. That is, cells with large charge endpoint capacity slippage during cycling normally have large voltage drops during storage. Fig. 2a shows that cells containing 2% VC + 2% TAP in SL:EMC electrolyte have much better storage performance than cells with 2% PES +1% MMDS +1% TTSPi in EC:EMC at 60. °C. Fig. 2b shows the coulombic efficiency (CE) vs. cycle number for NMC/graphite cells containing these two electrolyte systems during a cycling/storage protocol as explained in the experimental section. Fig. 2b shows that cells with 2% VC + 2% TAP in SL:EMC electrolyte had a similar CE to the cells with 2% PES +1% MMDS +1% TTSPi in EC:EMC electrolyte. Fig. 2c shows the impedance spectrum measured after UHPC cycling. The EIS measurements were made at 10 °C with a cell voltage of 3.80 V. The diameter of the semicircle represents the sum of the charge-transfer resistances, R_{ct}, at both the positive and negative electrodes. Smaller values of R_{ct} are desired for cells cycled for the same period of time. Fig. 2c shows cells containing 2% VC + 2% TAP in SL:EMC electrolyte have higher R_{ct} than cells containing 2% PES +1% MMDS +1% TTSPi in EC:EMC electrolyte. Fig. 2d shows the volume of gas evolved during the 600 h of UHPC cycling for the cells with the two electrolytes. Fig. 2d shows that cells containing 2% VC + 2% TAP in SL:EMC electrolyte produced more gas than 2% PES +1% MMDS +1% TTSPi in EC:EMC electrolyte.

Fig. 3a–b summarize V_{drop} during 500 h storage at 4.5 V at 60.°C and 40.°C, respectively, for NMC442/graphite pouch cells with different electrolyte additive combinations. Each data point in Fig. 3 represents the average of data from two cells and the error bars are the standard deviation of the results. The red bars in Fig. 3 represent cells containing EC:EMC electrolyte while the cyan bars in Fig. 3 represent cells containing SL:EMC electrolyte. When data is not available due to experiments not being conducted in some cases no bars are shown. Fig. 3a shows that the voltage drop for cells containing control or PES 211 in EC:EMC electrolyte system is roughly the same at 60.°C. NMC/graphite cells with control and

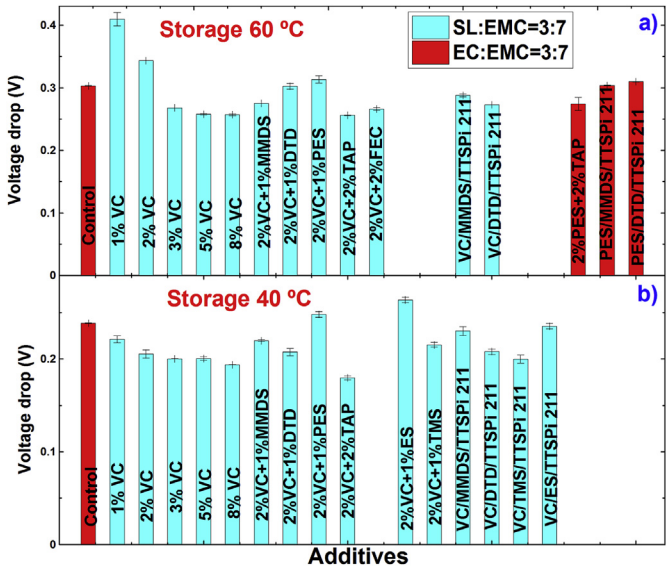

Fig. 3. Summary of V_{drop} during 500 h storage (4.5 V) at a) 60 °C and b) 40 °C for NMC442/graphite pouch cells incorporating SL:EMC electrolyte.

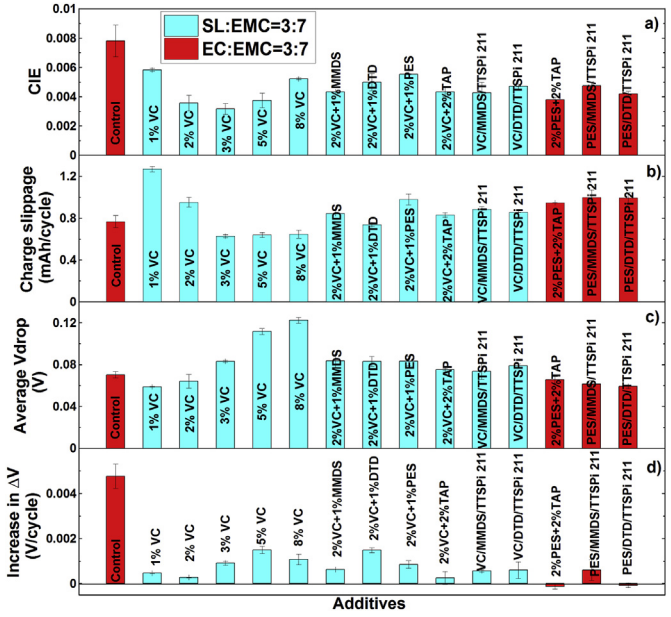

Fig. 4. Summary of cycling data collected on the UHPC including: CIE (CIE = 1 − CE), charge endpoint capacity slippage, V_{drop} and ΔV for NMC442/graphite pouch cells in SL:EMC electrolyte.

PES211 electrolyte do not show the same storage behavior at lower potentials [26]. For example at 4.2 V, PES211 shows much better storage properties than control electrolyte. This suggests that whatever film is formed by PES211 at the positive electrode/electrolyte interface is, itself, oxidized away when the potential is high enough. Fig. 3a shows that NMC/graphite cells with SL:EMC:2% VC have worse storage performance than control cells at 60.°C. However, adding other additives to the SL:EMC:2%VC electrolyte system generally improves the storage performance at 4.5 V and 60.°C. Fig. 3b shows that V_{drop} at 40.°C is smaller than that at 60.°C, indicating that the parasitic reactions during storage are temperature dependent. Fig. 3b shows that adding 2% PES or 1% ES to SL:EMC:2%VC electrolyte increase V_{drop} while adding 2% TAP decreases V_{drop} at 40.°C. Adding MMDS, DTD, TMS with or without TTSPi do not change in V_{drop} substantially at 4.5 V and 40.°C. In any event, adding TAP to SL:EMC:2% VC provides the cells with the best storage performance among the additives studied in this paper.

Fig. 4a summarizes the coulombic inefficiency (CIE = 1 − CE) for NMC442/graphite pouch cells with different electrolyte additives combination at 40. ± 0.1 °C. Detailed CE vs cycle number data are given in Figs. S3a, S4a and S5a in the supporting information. The CIE was calculated from the CE by taking an average of the final three data points (cycles 13–15) collected on the UHPC. Just as a reminder, smaller values of CIE means the cells had higher CE and should have a longer cycle and calendar life. Fig. 4a shows that all of the cells containing SL:EMC electrolyte have lower CIE (better) than that of control cells. Adding more additives to SL:EMC:2%VC electrolyte generally increased the CIE (lower CE = worse).

Fig. 4b summarizes the charge endpoint capacity slippage for NMC442/graphite pouch cells with different additives combinations at 40 ± 0.1 °C. Detailed charge endpoint capacity vs cycle number data are given in Figs. S3c, S4c and S5c in the supporting information. The charge endpoint capacity slippage was calculated from the slope of a best fit line to the final five points (cycles 11–15) of the charge endpoint capacity vs. cycle number curves. Fig. 4b shows adding more VC leads to lower charge end-capacity slippage rate in SL:EMC:2%VC electrolyte. Adding additives to SL:EMC:2%VC electrolyte decreases the charge end-capacity slippage rate except in cells containing 2%VC+2% PES, suggesting that 2%VC+2% PES is not an effective combination in the SL:EMC electrolyte system.

Compared with cells in the EC:EMC system, cells containing SL:EMC electrolyte generally have lower charge end point capacity slippage rates, indicating the beneficial effect of using SL instead of EC. It is extremely important to point out that charge endpoint capacity slippage for control cells is artificially small due to impedance growth (see Fig. S3f) causing severe capacity loss (Fig. S3b). In such a situation, the cell reaches the upper trip point earlier and earlier on successive cycles due to the increased "IR" drop which leads to an artificially small vale of the charge endpoint capacity slippage.

Fig. 4c–d summarize the average V_{drop} and the rate of increase of ΔV for the NMC442/graphite pouch cells with different additives combinations at 40 ± 0.1 °C during testing using the UHPC. Detailed V_{drop} and ΔV vs. cycle number data are given in Figs. S3e, S4e, S5e, S3f, S4f and S5f in the supporting information. The average V_{drop} was calculated from the data by taking an average of the final three data points (cycles 13–15) in the V_{drop} vs. cycle number curves collected on the UHPC. The rate of increase of ΔV was calculated from the slope of a best fit line to the final five points (cycles 11–15) of the ΔV vs. cycle number curves. The differences in V_{drop} from cell to cell are caused by differences in the rate of the electrolyte oxidation on the positive side and also by differences in DC resistance which affect the rapid voltage change when the cells switch from charge to open circuit [21]. This is not the case during 500 h storage since there is a holding process applied before the storage experiments. The increase in ΔV is caused by an increase in cell polarization during cycling and smaller values of increase in ΔV generally indicate lower impedance growth during cycling [30,38]. Fig. 4c shows that adding more VC or more additives to SL:EMC:2% VC electrolyte generally increased V_{drop} due to impedance increase. Fig. 4c shows that cells containing EC:EMC electrolyte had smaller V_{drop} than cells containing SL:EMC:2% VC electrolyte with additives. Fig. 4d shows that the control cells have much larger values of the increase in ΔV, indicating remarkable impedance growth during the last few cycles on the UHPC. Fig. 4d shows that cells containing 2% PES +1% DTD +1% TTSPi and 2% PES +2% TAP in EC:EMC electrolyte as well as 2% VC and 2% VC+2%TAP additive blends in SL:EMC electrolyte have very small impedance growth during the

UHPC cycling.

Fig. 5a–c show a summary of the EIS data after 600 h UHPC cycling at 40 °C (to 4.4 V, including a 20 h storage at 4.4 V each cycle) using the cycle/store protocol, after the 500 h storage test at 60.°C and 4.5 V, and after the 500 h storage test at 40.°C and 4.5 V, respectively. Impedance spectra for all of the cells tested in this study are given in Figs. S6 and S7. Fig. 5, S6 and S7 show that adding more VC to the SL:EMC:2%VC electrolyte system increased the impedance while adding MMDS decreased the impedance. Adding TAP to both SL:EMC and EC:EMC electrolyte systems greatly increased the impedance.

Fig. 6a, b, and 6c show the volume of gas produced during UHPC cycling, during the 500 h storage test at 60.°C and 4.5 V, and during the 500 h storage test at 40.°C and 4.5 V, respectively. Fig. 6a shows that adding more VC to the SL:EMC:2%VC electrolyte system increased the gas evolution. Fig. 6a also shows that cells containing EC:EMC electrolyte produce less gas than the SL:EMC electrolyte system during UHPC cycling. Fig. 6b–c shows that cells containing TAP in both SL:EMC and EC:EMC electrolyte systems had no gas problem at 60 ± 0.1 °C and 40 ± 0.1 °C.

Sulfolane does not form a stable SEI film on the graphite electrode and VC acts as a SEI forming electrolyte additive in the sulfolane:EMC system [21]. When either insufficient or excess VC is present in cells after formation, these cells can generate gas at high potential and at high temperature [22]. That is why the cells described in Fig. 6 all produced a large amount of gas during high temperature storage at 60 ± 0.1 °C except for the TAP-containing cells. It has been proposed that TAP can be easily polymerized at the surface of both graphite and coated NMC442 electrodes [29]. That is presumably why TAP-containing cells have high impedance

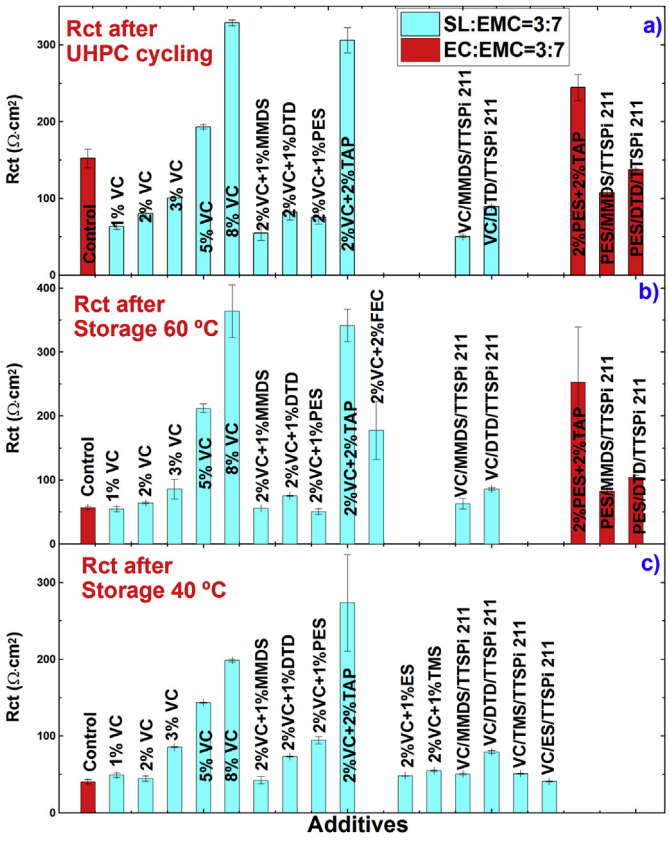

Fig. 5. Summary of the charge transfer resistance (R_{ct}) measured after a) UHPC cycling, b) 500 h storage at 60 °C (4.5 V) and c) 500 h storage at 40 °C (4.5 V) for NMC442/graphite pouch cells using SL:EMC electrolyte.

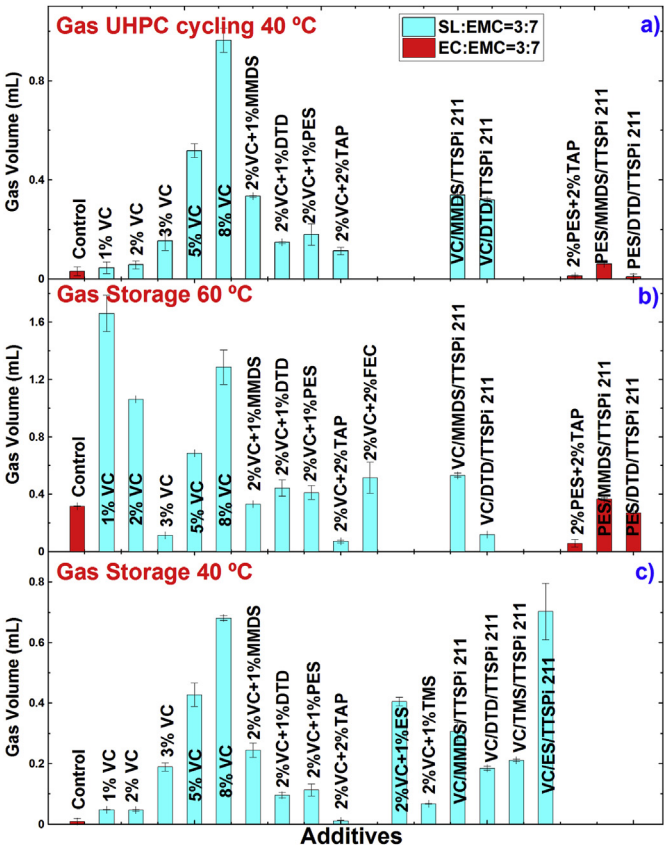

Fig. 6. Summary of the gas evolution measured during a) UHPC cycling, b) 500 h storage at 60 °C (4.5 V) and c) 500 h storage at 40 °C (4.5 V) for NMC442/graphite pouch cells using SL:EMC electrolyte.

at both NMC442 and graphite electrodes, which has been demonstrated by symmetric cell studies in Ref. [29]. The thick SEI films formed by TAP presumably decrease the parasitic electrolyte oxidation reactions between the charged electrode and the electrolyte and therefore decrease gas evolution and improves cycling and storage performance (eg. higher CE, lower charge endpoint capacity slippage during UHPC cycling and lower voltage drop during storage). Ternary additives blends that include VC, a sulfur-containing additive and TTSPi also reduce the rate of parasitic reactions on the positive electrode compared to VC alone, increase the thermal stability of the charged graphite electrode at elevated temperature, improve coulombic efficiency and also reduce impedance of the cells [39]. That may be why such ternary additives blends in the SL:EMC electrolyte perform much better than VC alone in the SL:EMC electrolyte (see Fig. 7). However, these ternary additive blends produce a large volume of gas during high temperature storage, which is the main disadvantage compared to TAP-containing cells in SL:EMC electrolyte.

Fig. 7a, c and e show the capacity vs. cycle number for the NMC442/graphite pouch cells containing different additives combinations in SL:EMC electrolyte. Fig. 7b, d and f show the difference between the average charge and discharge voltage (ΔV) vs. cycle number for the same cells shown in Fig. 7a, c and e, respectively. The long-term cycling cells were the same cells used for the UHPC cycling experiments and the long-term cycling began immediately after the UHPC cycling completed. All cells were continuously cycled with clamps to ensure firm pressure. Cells were cycled between 2.8 V and 4.5 V at 40 ± 0.5 °C using currents corresponding to C/2.5 (100 mA). Only one cell of each type is available due to the

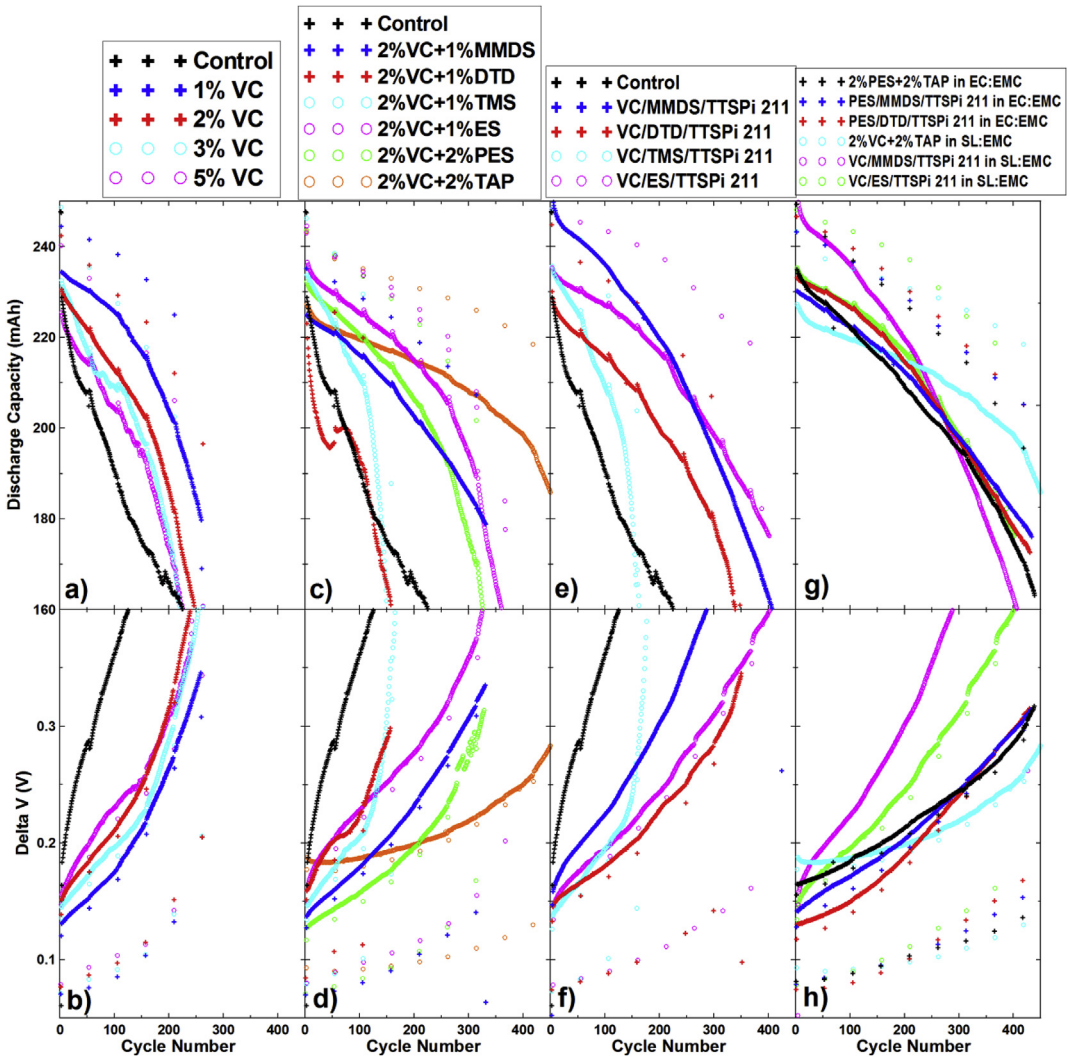

Fig. 7. a, c, e, g) Discharge capacity and b, d, f, h) ΔV, all plotted vs. cycle number for NMC442/graphite pouch cells using SL:EMC electrolyte with different additive sets as indicated. "Control" designates cells with 1 M $LiPF_6$ in EC:EMC 3:7. Panels g and h also contain data for cells with preferred electrolyte additives in EC:EMC. The cycling was between 2.8 and 4.5 V at C/2.4 (100 mA) at 40 ± 0.1 °C.

limited number of testing channels. Fig. 7a–b shows that adding more VC generally leads to worse capacity retention and larger ΔV during cycling. Fig. 7b shows adding TAP, ES, MMDS and PES leads to better cycling performance compared to cells containing SL:EMC:2%VC electrolyte. Fig. 7c shows adding TTSPi improves the cycling performance.

In previous studies, "PES-211" [14] and TAP [29] were shown to be beneficial in suppressing impedance growth in NMC442/graphite cells cycled up to 4.5 V. It is therefore meaningful to compare the results in the SL:EMC electrolyte system with results for cells containing "PES-211" or 2% TAP in 1 M $LiPF_6$ EC:EMC 3:7 electrolyte. Fig. 7g–h compare the discharge capacity as well as ΔV vs. cycle number for NMC442/graphite pouch cells containing some of the best additives combinations in SL:EMC:2% VC electrolyte to cells with "PES-211" or 2% PES +2%TAP in EC:EMC 3:7 electrolyte. Fig. 7g–h shows that cells containing 2% VC + 2% TAP in SL:EMC electrolyte have better capacity retention and less impedance growth during long-term cycling than cells with "PES-211" or 2% PES +2%TAP in EC:EMC 3:7. Astute readers may wonder if the improved cycling performance for SL:EMC with 2% VC + 2% TAP is actually caused by the high initial impedance in those cells (see Fig. 7h) which limits reduces the initial capacity and, hence, the exposure of the positive electrode to the highest potential. However, the storage data shown in Fig. 3a–b do indicate that cells using SL:EMC with 2% VC + 2% TAP do have the best storage performance and hence the smallest rates of electrolyte oxidation which is consistent with a smaller rate of impedance growth as seen in Fig. 7h.

Fig. 8a shows the cycle number when the cell discharge capacity reaches 180 mAh (~80% capacity retention) for NMC442/graphite pouch cells containing different additive combinations in SL:EMC and EC:EMC electrolyte. Fig. 8a shows that all of the SL:EMC-based electrolytes (except 2% VC+1% DTD) have better capacity retention than that of control cells. When compared with additives combinations such as PES 211 and 2% PES +2% TAP in EC:EMC electrolyte, only 2% VC+2% TAP in SL:EMC electrolyte provides better capacity retention. Figs. S8a and S8b (supporting information) show a summary of the gas produced after the entire long-term cycling test and impedance measurement at 3.8 V and at 10.°C after long-term cycling. Fig. S8 shows the additive blends which have better capacity retention generally have excellent gas control and impedance control during long-term cycling. However, 2% VC+2% TAP in SL:EMC electrolyte shows more gas generation and higher impedance than PES 211 and 2% PES +2%TAP in EC:EMC electrolyte after

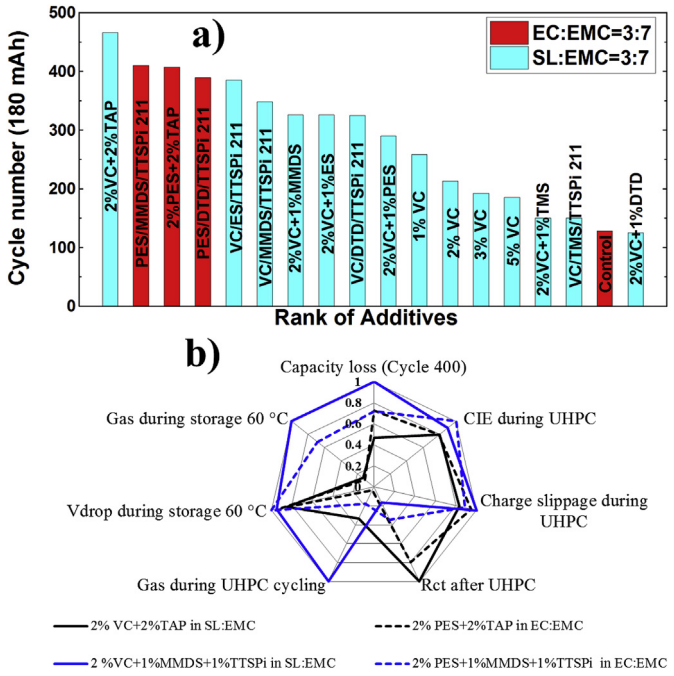

Fig. 8. a) The cycle number when the cell capacity reaches 180 mAh (80% retention) for NMC442/graphite pouch cells in SL:EMC electrolyte with different additive sets as indicated. Comparative data for cells with EC:EMC based electrolytes are also shown. The cycle number has been arranged from "best" at the left to "worst" at the right. b) A "radar" or "spider" plot which compares the best additive blends, based on the results in this work, in one graph. The seven axes represent the coulombic inefficiency, the charge endpoint capacity slippage, the charge transfer resistance after UHPC cycling, the gas volume during UHPC cycling, V_{drop} during storage at 60. ℃, the gas volume during storage at 60. ℃ and the capacity of cycle 400 during long term cycling. The axes have been scaled so that 100% is the value of the additive that has the largest (the worst) value of each parameter. The best additive blend would have values closest to the center of the plot.

the long-term cycling test.

Gas chromatography coupled with a thermal conductivity detector (GC-TCD) was used to analyse the different gases produced during storage. After the storage period, cells were discharged to 3.8 V for EIS measurements. Then cells were stored in a desk drawer at room temperature for about 1 year before the gas compositions were measured. It is very possible that some gases, especially CO_2 were consumed at the negative electrode during this time in the drawer. Thus, the gas compositions measured may not exactly reflect those in the cell immediately after the 40 °C and 60 °C storage periods. Fig. S9 shows that the main gaseous products during storage at 40 °C include H_2, CH_4, CH_3CH_3 and very small amounts of CO_2. The production of hydrogen is probably from the reduction of tiny amounts of water originally in the cell. CH_4 and C_2H_6 probably come from the reduction of EMC. CO_2 probably comes from the oxidation of VC or EMC. At 60 °C, the amounts of H_2 and CH_4 were greatly increased. One more gas produced during storage at 60 °C is CO, which is likely due to the oxidation of VC or EMC.

Fig. 8b shows a "radar" or "spider" plot which summarizes some of the best electrolyte additive combinations studied in this paper. The seven axes represent the capacity retention at cycle 400, CIE during UHPC testing, charge endpoint capacity slippage during UHPC testing, R_{ct} after UHPC testing, gas produced during UHPC testing, V_{drop} during storage at 60 °C (500 h, 4.5 V) and gas evolution during storage at 60 °C. The axes have been scaled so that 100% is the value of the additive that has the largest (the worst) value of each parameter among the 4 electrolytes presented. Therefore the best additive blend would have values closest to the center of the plot. Fig. 8b shows there is no obvious "winner" in all experiments amongst these additive blends. However, Fig. 8b does show that the cells containing 2% VC+2% TAP in SL:EMC electrolyte have lower CIE, lower charge slippage during UHPC cycling as well as lower gas and lower voltage drop during storage at 60 °C which may contribute to the best capacity retention during long-term cycling. One problem of 2% VC+2% TAP in SL:EMC electrolyte is its high impedance which may limit its high rate cycling performance. Tradeoffs between cycle life time and impedance would have to be made.

3.1. Summary and conclusions

SL:EMC:2% VC electrolyte with various additional electrolyte additives combinations was studied in NMC442/graphite pouch type Li-ion cells. The results of CE, charge endpoint capacity slippage, changes in ΔV and V_{drop} during UHPC cycle/store testing to 4.4 V and at 40 °C, V_{drop} during 500 h storage at 60 °C and 4.5 V, gas evolution, EIS, as well as long-term cycling results were considered and were compared to EC:EMC electrolytes with "PES211" or 2% PES+2%TAP electrolyte additive blends. The results showed that adding more VC, up to 3% VC, to the SL:EMC electrolyte system provided a beneficial effect in decreasing the electrolyte oxidation (lower voltage drop during storage) but adding 3% VC or more dramatically increased cell impedance (Fig. 5) and gassing (Fig. 6). This presumably caused the poor cycling behavior in Fig. 7a for cells with large amounts of VC. The cycling and storage performance of the SL:EMC:2% VC electrolyte system could be improved by adding electrolyte additives, especially 2% TAP. Comparing NMC/graphite cells with EC:EMC electrolyte containing "PES211" or 2% PES +2% TAP additive blends, SL:EMC electrolyte with 2%VC + 2%TAP provided smaller voltage drop during storage, similar CE and lower charge endpoint capacity slippage during UHPC cycling, lower gas evolution during storage at 4.5 V and 60 °C as well as better capacity retention during long-term cycling. However, cells containing SL:EMC electrolyte with 2% VC + 2% TAP display high impedance. This indicates that the SL:EMC:VC:TAP electrolyte system is deserving of further consideration including combinations with a third additive which could serve as an impedance reducer. Such studies are underway in our lab.

Acknowledgment

The authors acknowledge the financial support of NSERC and 3M Canada under the auspices of the Industrial Research Chairs program. The authors thank Dr. Jing Li of BASF for providing the most of the solvents and salts used in this work.

Appendix A. Supplementary data

Supplementary data related to this article can be found at http://dx.doi.org/10.1016/j.jpowsour.2016.06.008.

References

[1] J.B. Goodenough, Y. Kim, Chem. Mater. 22 (2010) 587.
[2] A. Manthiram, J. Phys. Chem. Lett. 2 (2011) 176.
[3] A. Kraytsberg, Y. Ein-Eli, Adv. Energy Mater. 2 (2012) 922.
[4] K. Amine, H. Yasuda, M. Yamachi, Electrochem. Solid State Lett. 3 (2000) 178.
[5] J. Wolfenstine, J. Allen, J. Power Sources 136 (2004) 150.
[6] J. Hadermann, A.M. Abakumov, S. Turner, Z. Ha, N.R. Khasanova, E.V. Antipov, G. Van Tendeloo, Chem. Mater. 23 (2011) 3540.
[7] B.H. Huang, S. Yin, T. Kerr, N. Taylor, L.F. Nazar, Adv. Mater. 14 (2002) 1525.
[8] J. Kim, S. Myung, C.S. Yoon, S.G. Kang, Y. Sun, Chem. Mater. 16 (2004) 906.
[9] Z. Lu, D.D. MacNeil, J.R. Dahn, Electrochem. Solid State Lett. 4 (2001) A200.
[10] L. Yang, B. Ravdel, B.L. Lucht, Electrochem. Solid State Lett. 13 (2010) A95.

[11] K. Xu, Chem. Rev. 114 (2014) 11503.
[12] Y. Wang, L. Xing, W. Li, D. Bedrov, J. Phys. Chem. Lett. 4 (2013) 3992.
[13] L.E. Downie, J.R. Dahn, J. Electrochem. Soc. 161 (2014) A1782.
[14] L. Ma, J. Xia, J.R. Dahn, J. Electrochem. Soc. 161 (2014) A2250.
[15] K.J. Nelson, G.L. Eon, A.T.B. Wright, L. Ma, J. Xia, J.R. Dahn, J. Electrochem. Soc. 162 (2015) 1046.
[16] K. Xu, C.A. Angell, J. Electrochem. Soc. 149 (2002) A920.
[17] A. Abouimrane, I. Belharouak, K. Amine, Electrochem. Comm. 11 (2009) 1073.
[18] X. Sun, C.A. Angell, Electrochem. Comm. 11 (2009) 1418.
[19] J. Xiang, F. Wu, R. Chen, L. Li, H. Yu, J. Power Sources 233 (2013) 115.
[20] N. Shao, X.-G. Sun, S. Dai, D. Jiang, J. Phys. Chem. B 115 (2011) 12120.
[21] J. Xia, J. Self, L. Ma, J.R. Dahn, J. Electrochem. Soc. 162 (2015) A1424.
[22] J. Xia, L. Ma, C.P. Aiken, K.J. Nelson, L.P. Chen, J.R. Dahn, J. Electrochem. Soc. 161 (2014) A1634.
[23] K.J. Nelson, J. Xia, J.R. Dahn, J. Electrochem. Soc. 161 (2014) A1884.
[24] J. Xia, N.N. Sinha, L.P. Chen, G.Y. Kim, D.J. Xiong, J.R. Dahn, J. Electrochem. Soc. 161 (2014) 84.
[25] J. Xia, N.N. Sinha, L.P. Chen, J.R. Dahn, J. Electrochem. Soc. 161 (2013) A264.
[26] D.Y. Wang, J. Xia, L. Ma, K.J. Nelson, J.E. Harlow, D. Xiong, L.E. Downie, R. Petibon, J.C. Burns, a. Xiao, W.M. Lamanna, J.R. Dahn, J. Electrochem. Soc. 161 (2014) A1818.
[27] J. Xia, L. Ma, J.R. Dahn, J. Power Sources 287 (2015) 377.
[28] L. Ma, D.Y. Wang, L.E. Downie, J. Xia, K.J. Nelson, N.N. Sinha, J.R. Dahn, J. Electrochem. Soc. 161 (2014).
[29] J. Xia, L. Madec, L. Ma, L.D. Ellis, W. Qiu, K.J. Nelson, Z. Lu, J.R. Dahn, J. Power Sources 295 (2015) 203.
[30] J. Xia, Z. Lu, J. Camardese, J.R. Dahn, J. Power Sources 306 (2016) 516.
[31] T.M. Bond, J.C. Burns, D. a. Stevens, H.M. Dahn, J.R. Dahn, J. Electrochem. Soc. 160 (2013) A521.
[32] N.N. Sinha, T.H. Marks, H.M. Dahn, a. J. Smith, J.C. Burns, D.J. Coyle, J.J. Dahn, J.R. Dahn, J. Electrochem. Soc. 159 (2012) A1672.
[33] C.P. Aiken, J. Xia, D.Y. Wang, D. a. Stevens, S. Trussler, J.R. Dahn, J. Electrochem. Soc. 161 (2014) A1548.
[34] R. Petibon, C.P. Aiken, N.N. Sinha, J.C. Burns, H. Ye, C.M. VanElzen, G. Jain, S. Trussler, J.R. Dahn, J. Electrochem. Soc. 160 (2012) A117.
[35] D.Y. Wang, A. Xiao, L. Wells, J.R. Dahn, J. Electrochem. Soc. 162 (2014) A169.
[36] J. Self, C.P. Aiken, R. Petibon, J.R. Dahn, J. Electrochem. Soc. 162 (2015) A796.
[37] J. Xia, M. Nie, L. Ma, J.R. Dahn, J. Power Sources 306 (2016) 233.
[38] J.C. Burns, X. Xia, J.R. Dahn, J. Electrochem. Soc. 160 (2012) A383.
[39] L. Ma, D.Y. Wang, L.E. Downie, J. Xia, K.J. Nelson, N.N. Sinha, J.R. Dahn, J. Electrochem. Soc. 161 (2014) A1261.